

# Long Term X-Ray Spectral Variation of the Wolf-Rayet Binary WR 102-1 in the Galactic bulge: evidence for wind distortion in the binary

Tomoki Nagatsuka,<sup>1,2\*</sup> Yasuharu Sugawara,<sup>1</sup> Ken Ebisawa,<sup>1,2</sup>

<sup>1</sup>*Institute of Space and Astronautical Science(ISAS), Japan Aerospace Exploration Agency(JAXA), 3-1-1 Yoshinodai, Chuo-ku, Sagami-hara, Kanagawa, 252-5210, Japan*

<sup>2</sup>*Department of Astronomy, Graduate School of Science, The university of Tokyo, 7-3-1 Hongo, Bunkyo-ku, Tokyo 113-0033, Japan*

Accepted XXX. Received YYY; in original form ZZZ

## ABSTRACT

WR 102-1 was detected by *Suzaku* as a conspicuous point source in the 6.7 keV intensity map of the central region of the Milky Way. The source was suggested as a possible Wolf-Rayet binary based on its X-ray and infrared spectral characteristics. The iron line emission is expected to originate in the Wolf-Rayet star's dynamic stellar-wind when colliding the companion's mild stellar wind. Here, we report the result of a long-term X-ray monitoring of WR 102-1 since 1998 using archival data of *ASCA*, *XMM-Newton*, *Chandra*, *Suzaku*, and *Swift* to reveal variations of the iron K-emission line and the circumstellar absorption. Consequently, we have detected significant redshifts of the iron K-emission line from the *XMM-Newton* observation in March 2003 and the *Suzaku* observation in September 2006. Furthermore, when the red-shift was observed, which suggests that the Wolf-Rayet star was in front of the companion star, the circumstellar absorption values were smaller than other periods. These results appear contrary to the expectation if the Wolf-Rayet's stellar wind is spherically symmetric, but may be understood if the Wolf-Rayet star's stellar wind is significantly distorted due to the rapid orbital motion near the periastron.

**Key words:** stars: Wolf-Rayet — X-rays: Individual: WR 102-1 — binaries: spectroscopic

## 1 INTRODUCTION

Wolf-Rayet (WR) stars are luminous hot stars exhibiting broad emission lines, and considered to be in the final stage of the stellar evolution of massive stars with  $\gtrsim 25 M_{\odot}$  (e.g., [Rosslowe & Crowther 2015](#)). Most WR stars are ejecting strong stellar winds (e.g., [Meynet & Maeder 2005](#)), and a significant fraction of the WR stars are in binaries ([van der Hucht 2001](#); [Neugent et al. 2014](#)). O-type stars also often emit stellar winds and are found in binaries ([Sana et al. 2012](#)). In those WR binaries with stellar-wind emitting companions, wind-wind collisions are expected, which would exhibit intriguing astrophysical phenomena.

In the WR binaries with O- or B-type companions, shock waves are generated when the WR star's strong stellar wind collides violently with the companion star's milder stellar wind. This heats up the plasma hot enough to emit X-rays. The X-ray luminosity and energy spectrum are highly dependent on the circumstellar distance, mass-loss rates, and velocities of the stellar winds. Thus, X-ray spectral analysis can reveal these physical parameter variations with the orbital phase (e.g., [Sugawara et al. 2015](#)). In addition, Doppler shift of the emission lines, if detected, would reveal dynamics of the stellar winds.

A bright point object was discovered in the 6.7 keV intensity map of the central region of the Milky Way by *Suzaku*, and the source was suggested as a possible WR binary from its X-ray and infrared characteristics ([Hyodo et al. 2008](#)). The source was also detected

by *Chandra*<sup>1</sup> and *XMM-Newton*<sup>2</sup>, designated as CXOU J174645.2–281547/4XMM J174645.2–281548, and listed in the Wolf-Rayet catalog by [Rate et al. \(2020\)](#) as WR 102-1<sup>3</sup>.

Because WR 102-1 is located near the Galactic Center at the Galactic coordinates  $(l, b)=(0.70480, 0.13723)$ , the source has been often serendipitously in the fields of view of the pointing observations targeting the Galactic Center. We have found 11 observations in total by *XMM-Newton*, *Chandra*, and *Suzaku* from September 2000 to April 2018, for a total of 358 ksec exposure. Furthermore, WR 102-1 was in the field of view of five *ASCA* observations carried out from October 1993 to September 1998, and 46 observations by *Swift* from May 2007 to November 2020. Using these datasets, we have studied long-term variations of X-ray spectra and circumstellar environments of WR 102-1.

In Section 2, we present observations and data reduction. Data analysis and results are given in Section 3. Section 4 is the discussion, based on our finding of intriguing variations of the iron K-line emission.

## 2 OBSERVATION AND DATA REDUCTION

Table 1 shows the observation log by *Suzaku*, *Chandra* and *XMM-Newton* between September 2000 and April 2018. There were 11 observations of about 358 ksec in total. We also show angular distance

<sup>1</sup> <https://cxc.cfa.harvard.edu/csc/>

<sup>2</sup> <http://xmm-catalog.irap.omp.eu/>

<sup>3</sup> <http://pacrowther.staff.shef.ac.uk/WRcat/>

\* E-mail: nagatsuka@ac.jaxa.jp

**Table 1.** *XMM*, *Chandra* and *Suzaku* Observation log.

Satellite/Abbreviation	Detector	Obs.ID	Start Time(UT)	Exposure time (ks)	off-axis angle* (arcmin)
XMM1	PN,MOS1,MOS2	0112970201	2000/09/23 22:37	12.3	11.7
Chandra1	ACIS-S	1036	2000/10/27 11:27	35.0	10.5
XMM2	PN,MOS2	0112971501	2001/04/01 07:27	14.3	13.4
Chandra2	ACIS-I	2271	2001/07/16 05:34	10.4	9.5
	ACIS-I	2274	2001/07/16 08:43	10.4	5.7
	ACIS-I	2285	2001/07/16 18:08	10.4	7.9
XMM3	PN,MOS1,MOS2	0144220101	2003/03/12 17:54	31.7	10.4
Suzaku	XIS	501040010	2006/09/21 17:29	61.4	7.4
	XIS	501040020	2006/09/24 05:03	44.9	7.4
XMM4	MOS1,MOS2	0764190101	2016/03/10 08:51	32.5	13.1
XMM5	PN,MOS1,MOS2	0802410101	2018/04/02 00:59	95.0	10.7

\* Angular distance of the source from the optical axis.

**Table 2.** *ASCA*/*GIS* Observation log.

Obs.ID	Start Time(UT)	Exp. time (ks)	off-axis angle* (arcmin)
60001100	1993/10/01 21:35	17.5	17.5
52006000	1994/09/22 03:46	58.4	12.7
52006001	1994/09/24 02:07	21.5	12.7
54001000	1996/09/19 15:55	11.2	19.0
56001100	1998/09/07 15:01	10.0	21.1

\* Angular distance of the source from the optical axis.

of the source from the telescope bore-sights for each observation. In addition to the datasets used by [Hyodo et al. \(2008\)](#), this study includes two new observations of *XMM-Newton* in March 2016 and April 2018 (XMM 4 and 5 in Table 1) with a total of 127 ksec. In addition, we use *ASCA*/*GIS* and *Swift*/*XRT* archival data, where WR102-1 were coincidentally in the fields of view. The logs of these observations are shown in Table 2 and 3.

Although the source is located in a crowded region of variable sources near the Galactic Center, we found no significant contamination from nearby bright sources in these observations. Thus, we simply extracted the source events from the region centering around the source position in the following analysis.

## 2.1 *Suzaku*

X-ray Imaging Spectrometer (XIS; [Koyama et al. 2007](#)) on-board *Suzaku* consists of four X-ray CCD cameras (XIS-0, XIS-1, XIS-2, XIS-3). Together with the X-ray telescope ([Serlemitsos et al. 2007](#)), the energy range is 0.2–12 keV. XIS-0, 2 and 3 hold front-illuminated (FI) CCDs and only XIS-1 carries a back-illuminated (BI) CCD. The XIS data were reduced with HEASOFT version 6.26 ([NASA/HEASARC 2014](#)), following the *Suzaku* data analysis guide<sup>4</sup>. We used `xselect` to extract the data products from the cleaned event files where background events had been already removed. The source extraction region was a 20 arcsec radius circle, and the background was taken from a 60 arcsec circle in a nearby blank field. The response functions were calculated by `xisrmfgen`

<sup>4</sup> <https://heasarc.gsfc.nasa.gov/docs/suzaku/analysis/abc/>

**Table 3.** *Swift*/*XRT* Observation log.

Abbreviation	Obs.ID	Start Time (UT)	Exp. time (ks)	off-axis angle* (arcmin)
Swift1	00030938001	2007/05/13 15:33	4.5	6.8
	00030938002	2007/05/16 23:59	1.4	7.7
	00030938003	2007/07/03 16:17	1.4	3.9
Swift2	00030938004	2007/08/08 03:25	2.0	7.6
	00030938025	2019-05-13 04:14	2.2	7.6
	00030938026	2019-05-27 18:46	3.0	10.3
	00030938027	2019-06-10 18:50	3.3	9.0
	00030938028	2019-06-24 10:58	3.0	9.6
	00030938029	2019-07-08 09:46	2.8	7.3
	00030938031	2019-07-25 14:27	1.1	7.3
	00030938032	2019-07-26 08:12	1.2	9.3
	00030938033	2019-08-05 04:02	3.0	5.9
	00030938034	2019-08-20 12:17	3.0	7.5
Swift3	00030938035	2019-09-02 02:46	3.0	5.7
	00030938036	2020-02-04 13:13	2.8	8.1
	00030938037	2020-03-04 16:49	2.7	9.9
	00030938038	2020-04-03 02:46	2.8	6.2
	00030938039	2020-05-04 10:49	2.7	11.7
	00030938040	2020-06-04 01:31	2.8	9.4
	00030938041	2020-07-06 03:19	2.8	6.3
00030938042	2020-08-04 03:25	2.7	7.5	
00030938043	2020-09-04 03:49	3.0	7.0	

\* Angular distance of the source from the optical axis.

and `xisarfgen` ([Ishisaki et al. 2007](#)). Different FI CCD data were combined because they have almost identical performances.

## 2.2 *Chandra*

The *Chandra* satellite ([Weisskopf et al. 2001](#)) is equipped with an X-ray telescope with a high angular resolution of 0.5 arcsecond. We used Advanced CCD Imaging Spectrometer (ACIS), which consists of 10 CCDs; 2 × 2 square array of ACIS-I and 1 × 6 serial array of ACIS-S. Two of the ACIS-S CCDs are BI and the other eight are FI. WR 102-1 was observed by ACIS-S on 27 October 2000 ("Chandra1" in Table 1), and by ACIS-I on 16 July 2001 ("Chandra2"). All the ACIS observations were conducted in the Faint mode.

*Chandra* data was analyzed with CIAO version 4.11 ([Fruscione et al. 2006](#)) using the Level 1 mask file with PHA filtering. The source light curves were checked to confirm that there

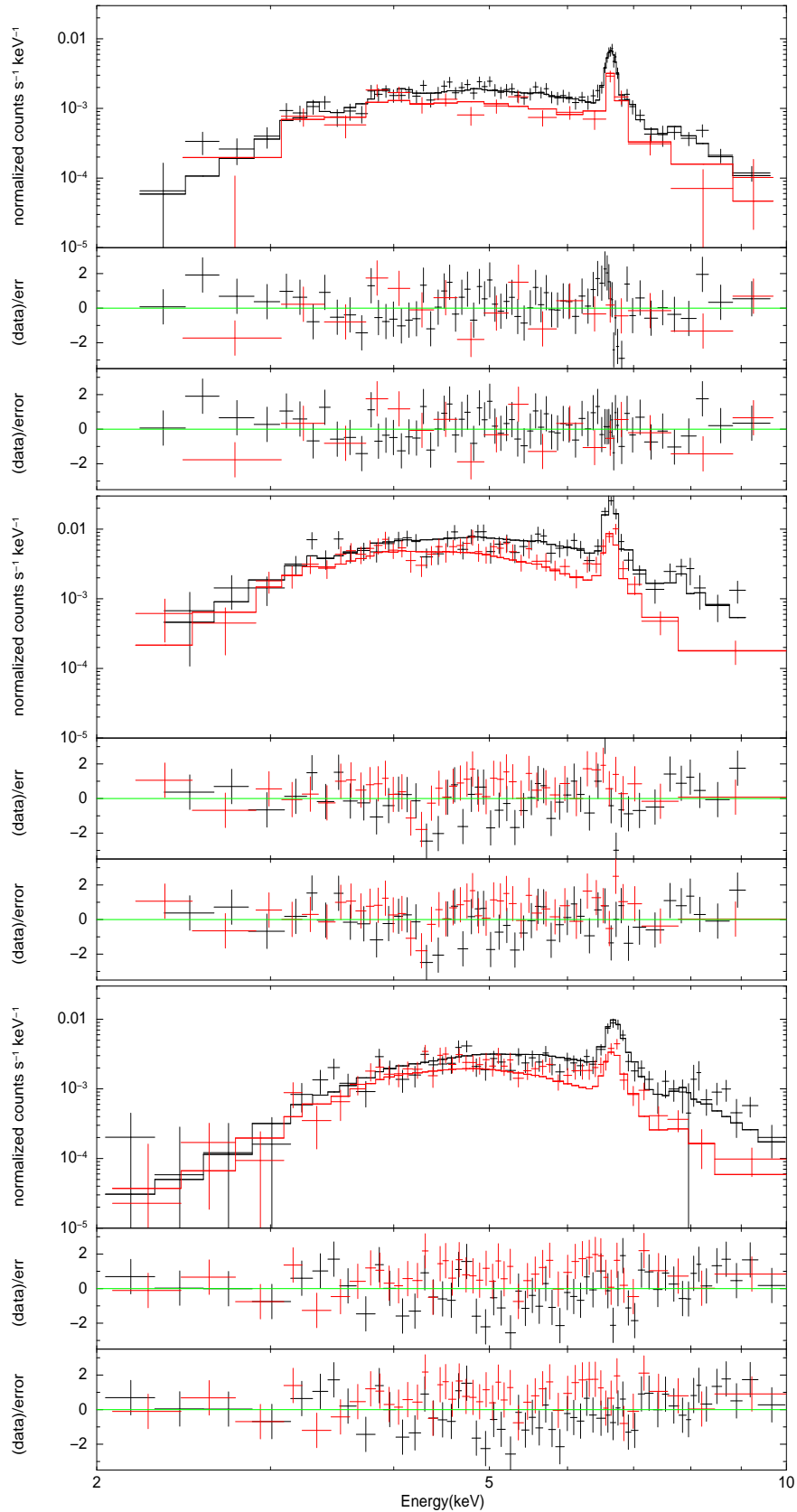


**Figure 1.** Spectral fitting results of WR 102-1 for Suzaku (top; black for FI, red for BI), XMM3 (middle; black for PN, red for MOS1+2), and XMM5 (bottom; same colors as for XMM3). In each of the three figures, the upper-panel gives the observed spectra and best-fit models, the middle-panel gives the residual when the red-shift and the turbulent velocity are null, and the bottom-panel is the residual with the best-fit red-shifts and turbulent velocities.

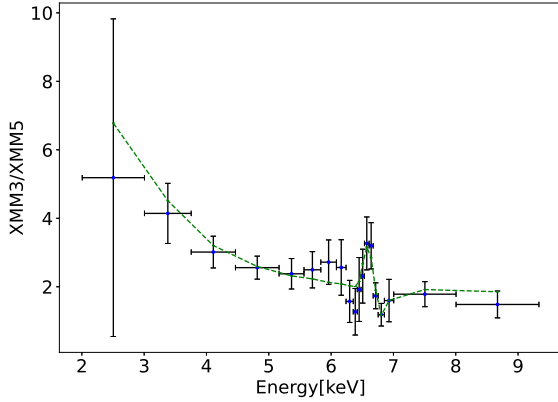


**Figure 2.** Spectral ratio of XMM3 to XMM5 (black). The green line shows the ratio of the best-fit model spectra in Table 2.

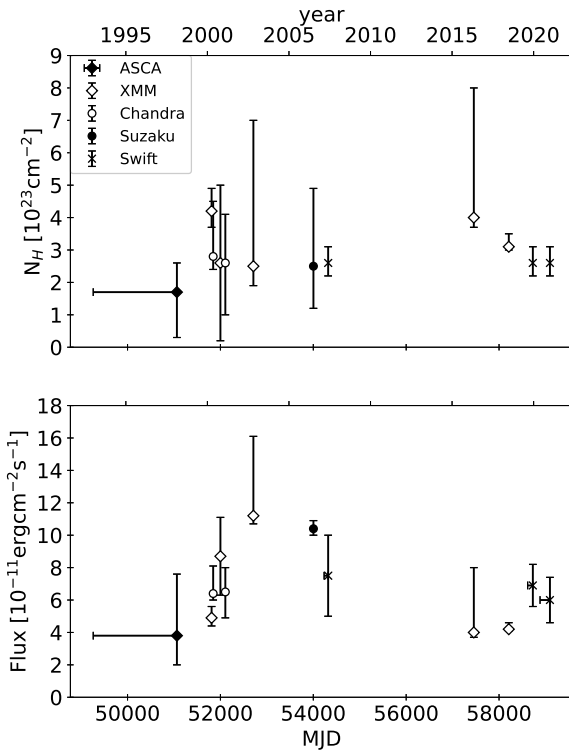


**Figure 3.** Variation of the X-ray flux (upper-panel) and the absorption hydrogen column density (lower-panel) by *ASCA*, *Suzaku*, *XMM*, *Chandra* and *Swift*/XRT.

were no background flares. We used *specextract* to extract the spectra. The source region was  $\sim 5$  arcsec radius and the background area was  $\sim 15$  arcsec radius in a nearby blank field.

### 2.3 XMM-Newton

For *XMM-Newton* (Jansen et al. 2001), we used EPIC, which is composed of two front-illuminated CCD cameras (MOS1 and MOS2) and

a back-illuminated camera (PN). Among the five XMM observations in Table 1, WR 102-1 was out of the field of view of MOS1 in the observation of 1 April 2001 ("XMM2") and out of the field of view of PN in the observation of 10 March 2016 ("XMM4"). All the observations were carried out with the Medium filter. The data were reduced with SAS version 17.0.0 (Gabriel et al. 2004), and *evselect* was used to obtain the filtered event files for EPIC-MOS1, 2 and PN in 0.3–10.0 keV. Light-curves were created with *evselect* and the GTI file was made with *tabgtigen*. Background flares were checked and removed. The source area was  $\sim 30$  arcsec radius and the background area was  $\sim 90$  arcsec radius in a nearby blank field. MOS1 and MOS2 spectra and responses were combined with *epicspeccombine*, and PN and MOS spectra were fitted simultaneously.

### 2.4 ASCA

The *ASCA* observation log is shown in Tables 2. Since the source flux was near the detection limit, we merged all the five observations carried out between October 1993 and September 1998, and combined the GIS2 and GIS3 counters. We used HEASOFT version 6.26, and *xselect* to extract the data products from the cleaned event files where the background events had been already removed. The source area was taken as  $\sim 140$  arcsec radius and the background was  $\sim 400$  arcsec radius in a nearby blank field.

### 2.5 Swift

The *Swift* observation log is shown in Table 3. We selected the *Swift*-XRT data whose center positions are within 15 arcmin from WR102-1 and the exposure times exceeding 1,000s. We produced the *Swift*-XRT light-curves and spectra using the *Swift*-XRT data product generator (Evans et al. 2007, 2009).<sup>5</sup> We combined the snap-shot observations carried out in 2007, 2019, and 2020, and created the three datasets (the first column in Table 3).

## 3 DATA ANALYSIS AND RESULTS

We created the energy spectra and responses of *XMM*, *Chandra*, *Suzaku*, and *Swift*XRT according to the first column of Table 1 and 3. These energy spectra were binned at a minimum of 15 counts per new bin for spectral fitting.

The spectral fitting was performed with *xspec* package (Arnaud 1996) using the *tbabs* absorption model by Wilms et al. (2000) and optically thin thermal plasma model *bvapec* (Smith et al. 2001). We adopted the Chi-Squared statistics and the solar abundances by Anders & Grevesse (1989). The heavy element abundance ratios were fixed to the ones determined previously by *Suzaku* and *XMM* analysis (Table 2 in Hyodo et al. 2008).

The three spectra, *Suzaku*, XMM3 and XMM5 have long enough exposures and high photon statistics to enable detailed spectral analysis. For these spectra, we carried out model fitting allowing all the parameters free, including the plasma red-shifts and turbulent velocities. We show the spectral fitting results for these spectra in Figure 1. In each spectrum, the top panel shows the spectra and the best-fit models. The middle panel is the residual of the model fit with the red-shifts and turbulent velocities being null, where we found residuals at around the iron emission line. If we allow the plasma red-shifts and turbulent velocities to be free, the residuals disappear (bottom

<sup>5</sup> [https://www.swift.ac.uk/user\\_objects/](https://www.swift.ac.uk/user_objects/)

panels in Figure 1). For Suzaku and XMM3, significant red-shifts are recognized, and there is a hint of blue-shift in XMM5. Best-fit parameters are shown in Table 2.

Figure 2 shows the spectral ratio of XMM3, which shows a clear energy red-shift, to XMM5, which shows a hint of blue-shift. From this figure, changes of the line centroid energy is clearly recognized. Furthermore, this figure, as well as Table 2, indicates that the low-energy absorption is less significant in XMM3, when the iron emission line is red-shifted. Possible origin of this is discussed in the next section.

For other spectra, rather low photon statistics does not allow to constrain the red-shift and turbulent velocities, thus we made these parameters null. In addition, for the spectra with low photon statistics in which the hydrogen column density or temperature were not constrained (XMM2, Swift 1, 2 and 3), they were fixed to the average values of Suzaku, XMM3 and XMM5.

Table 4 lists the best-fit parameter values and 90% confidence intervals. XMM2 and Swift1, 2, and 3 were fixed at the average of the best-fit values of Suzaku, XMM3, and XMM5, which have high photon statistics. Figure 3 shows the long-term variations of the absorbed flux and hydrogen column densities. We see the source has been visible for the entire period from early 1990's to 2020. The absorbed flux is variable by a factor of 2 to 3, and the column density is also significantly variable.

## 4 DISCUSSION

We have carried out a long-term X-ray spectral study of WR 102-1 using *ASCA*, *Suzaku*, *Chandra*, *XMM* and *Swift*/XRT. As a result, we have confirmed significant variation of the X-ray flux, low-energy absorption, and, in particular, iron line profile over two decades. In this section we discuss interpretation of these variations based on simple assumptions.

First assumption is that an increase of the soft X-ray absorption suggests an increase of the WR stellar wind density in the line-of-sight. Next, the X-ray luminosity due to the stellar wind-wind collision is expected to vary along with the binary separation according to the inversely proportional relation (Usov 1992). Thus, dimming the X-ray radiation suggests increase of the binary separation. Finally, X-rays are considered to be emitted from the cone-shape bow shock, which takes place when the WR star's strong stellar wind collides the O-star's milder stellar wind, so that the flow direction at the bow shock is from the WR star to the companion star. Motion of the X-ray emitting plasma flow at the bow shock results in the spectral line broadening and the energy shift.

From these interpretations, the binary geometries at Suzaku, XMM3 and XMM5 observations may be as shown in Figure 4. In Suzaku and XMM3 (upper-panel), the binary separation is smaller thus the X-ray luminosity is higher. The WR-star is in front of the companion star and the plasma flow at the bow shock is receding, thus the iron line red-shifts are seen. The WR star's wind is significantly distorted (see below). In XMM5 (lower-panel), the binary separation is larger, and the WR stellar wind is closer to spherically symmetric, as it is not significantly affected by the binary motion. X-rays are more significantly absorbed by the WR star's wind.

It is known that the binary stellar wind is significantly distorted near the periastron because of the proximity of the stars and the rapid orbital motion (e.g., Okazaki et al. 2008). In particular, a "hole" may be produced in the WR star's stellar wind. If we are observing the X-rays from the bow shock through the hole in the stellar wind (Figure 4 top), the soft X-ray absorption will be less significant.

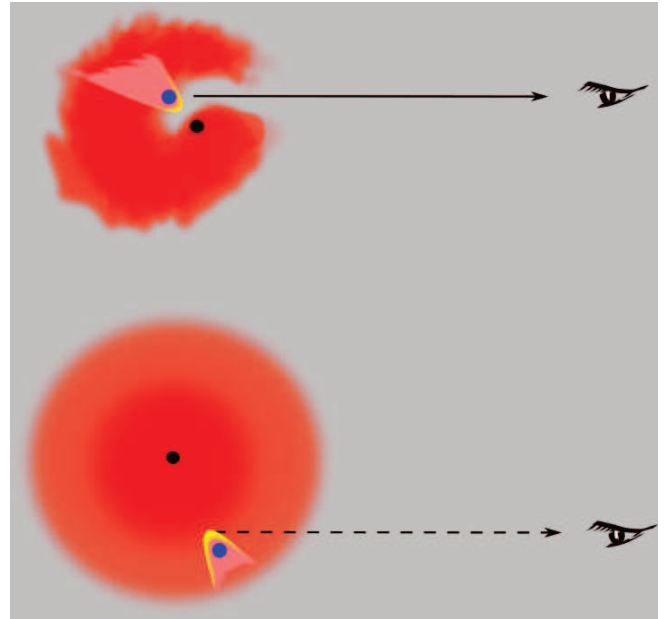


**Figure 4.** A possible binary geometry of WR 102-1. The black point is the WR star, the blue point is the companion star, and the red region denotes the stellar wind from the WR star. The X-rays are emitted from the cone-shape bow shock (yellow), which takes place when the WR star's strong stellar wind collides the milder stellar wind from the O-star, so that the flow at the bow shock is from the WR star to the companion star. Upper panel is for Suzaku and XMM3, when the clear red-shifts are seen, the fluxes are higher and the soft X-ray absorptions are less, and the bottom-panel is for XMM5, when there is a hint of blue-shift, the flux is lower, and the X-rays are more absorbed.

Hyodo et al. (2008) suggested that WR 102-1 may be a WC+O colliding wind binary with an elliptical orbit. Our results not only support their models, but also suggest that WR 102-1 is a long-period binary with a period of at least 10 years. We believe that continuous X-ray monitors over the next years will help prove this hypothesis.

## 5 DATA AVAILABILITY

The data analyzed in this research are all available at HEASARC of NASA<sup>6</sup> and DARTS of ISAS/JAXA.<sup>7</sup>

## 6 ACKNOWLEDGEMENTS

This research has made use of data, software and web tools obtained from the High Energy Astrophysics Science Archive Research Center (HEASARC), a service of the Astrophysics Science Division at NASA/GSFC and of the Smithsonian Astrophysical Observatory's High Energy Astrophysics Division. This research also made use of data obtained from Data ARchives and Transmission System (DARTS), provided by Center for Science-satellite Operation and Data Archive (C-SODA) at ISAS/JAXA. This research made use of data supplied by the UK Swift Science Data Centre at the University of Leicester. We acknowledge the use of public data from the Swift data archive. Based on observations obtained with *XMM-Newton*,

<sup>6</sup> <https://heasarc.gsfc.nasa.gov>

<sup>7</sup> <https://darts.isas.jaxa.jp>

**Table 4.** Best-fit parameters of the spectral fitting.

Observation	$N_{\text{H}}$ [ $10^{23}$ cm $^{-2}$ ]	kT [keV]	Red Shift $10^{-3}$	Velocity [km s $^{-1}$ ]	Flux@2.0-8.0keV [ $10^{-13}$ ergs cm $^{-2}$ s $^{-1}$ ]	$\chi^2/\text{dof}$
ASCA	1.7 $^{+2.5}_{-0.9}$	1.1 $^{+1.4}_{-0.7}$	–	–	3.8 $^{+1.8}_{-3.8}$	161.5/101
XMM1	4.2 $^{+0.8}_{-0.6}$	6.0 $^{+1.7}_{-1.5}$	–	–	4.9 $^{+0.5}_{-0.7}$	53.48/31
Chandra1	2.8 $\pm$ 0.4	6.5 $^{+6.1}_{-2.5}$	–	–	6.4 $^{+0.4}_{-1.7}$	14.6/13
XMM2	(2.6)*	(4.3)*	–	–	8.7 $^{+2.4}_{-2.4}$	0.69/3
Chandra2	2.6 $\pm$ 0.5	5.9 $^{+3.4}_{-2.4}$	–	–	6.5 $^{+1.6}_{-1.5}$	11.2/14
XMM3	2.5 $^{+0.6}_{-0.4}$	3.6 $^{+1.6}_{-1.4}$	5.3 $^{+5.8}_{-5.3}$	3300 $\pm$ 2700	11.2 $^{+0.5}_{-4.9}$	46.5/57
Suzaku	2.5 $^{+0.6}_{-0.4}$	3.6 $^{+1.6}_{-1.4}$	5.1 $\pm$ 1.5	300 $^{+1700}_{-300}$	10.4 $^{+0.4}_{-0.5}$	64.7/82
Swift1	(2.6)*	(4.3)*	–	–	7.5 $\pm$ 2.5	0.49/1
XMM4	4.0 $^{+1.4}_{-1.1}$	4.8 $^{+3.1}_{-2.2}$	–	–	4.0 $^{+0.3}_{-4.0}$	16.5/13
XMM5	3.1 $^{+0.2}_{-0.3}$	4.9 $\pm$ 0.8	–0.1 $^{+3.3}_{-3.1}$	3200 $\pm$ 1200	4.2 $^{+0.1}_{-0.4}$	126.8/102
Swift2	(2.6)*	(4.3)*	–	–	6.9 $\pm$ 1.3	6.87/6
Swift3	(2.6)*	(4.3)*	–	–	6.0 $\pm$ 1.4	5.25/4

\* Those values in the parentheses are fixed at the average of the best-fit values of Suzaku, XMM3, and XMM5.

an ESA science mission with instruments and contributions directly funded by ESA Member States and NASA. We thank Ms. Juriko Ebisawa for the artwork of Figure 4.

## REFERENCES

- Anders E., Grevesse N., 1989, *Geochimica Cosmochimica Acta*, **53**, 197
- Arnaud K. A., 1996, in Jacoby G. H., Barnes J., eds, *Astronomical Society of the Pacific Conference Series Vol. 101, Astronomical Data Analysis Software and Systems V*. p. 17
- Evans P. A., et al., 2007, *Astronomy and Astrophysics*, **469**, 379
- Evans P. A., et al., 2009, *Monthly Notices of the Royal Astronomical Society*, **397**, 1177
- Fruscione A., et al., 2006, in Silva D. R., Doxsey R. E., eds, *Society of Photo-Optical Instrumentation Engineers (SPIE) Conference Series Vol. 6270, Society of Photo-Optical Instrumentation Engineers (SPIE) Conference Series*. p. 62701V, doi:10.1117/12.671760
- Gabriel C., et al., 2004, in Ochsenein F., Allen M. G., Egret D., eds, *Astronomical Society of the Pacific Conference Series Vol. 314, Astronomical Data Analysis Software and Systems (ADASS) XIII*. p. 759
- Hyodo Y., Tsujimoto M., Koyama K., Nishiyama S., Nagata T., Sakon I., Murakami H., Matsumoto H., 2008, *Publications of the Astronomical Society of Japan*, **60**, S173
- Ishisaki Y., et al., 2007, *Publications of the Astronomical Society of Japan*, **59**, 113
- Jansen F., et al., 2001, *Astronomy & Astrophysics*, **365**, L1
- Koyama K., et al., 2007, *Publications of the Astronomical Society of Japan*, **59**, S23
- Meynet G., Maeder A., 2005, *A&A*, **429**, 581
- NASA/HEASARC 2014, HEASoft: Unified Release of FTOOLS and XANADU, Astrophysics Source Code Library, record ascl:1408.004 (ascl:1408.004)
- Neugent K. F., Massey P., Neugent K. F., Massey P., 2014, *ApJ*, **789**, 10
- Okazaki A. T., Owocki S. P., Russell C. M. P., Corcoran M. F., 2008, *MNRAS*, **388**, L39
- Rate G., Crowther P. A., Parker R. J., 2020, *Monthly Notices of the Royal Astronomical Society*, **495**, 1209
- Rosslove C. K., Crowther P. A., 2015, *Monthly Notices of the Royal Astronomical Society*, **447**, 2322
- Sana H., et al., 2012, *Science*, **337**, 444
- Serlemitsos P. J., et al., 2007, *Publications of the Astronomical Society of Japan*, **59**, 9
- Smith R. K., Brickhouse N. S., Liedahl D. A., Raymond J. C., 2001, *The Astrophysical Journal*, **556**, L91
- Sugawara Y., et al., 2015, *PASJ*, **67**, 121
- Usov V. V., 1992, *The Astrophysical Journal*, **389**, 635
- Weisskopf M. C., Brinkman B., Canizares C., Garmire G., Murray S., Speybroeck L. P. V., 2001, *Publications of the Astronomical Society of the Pacific*, **114**, 1
- Wilms J., Allen A., McCray R., 2000, *ApJ*, **542**, 914
- van der Hucht K. A., 2001, *VizieR Online Data Catalog*, p. III/215

This paper has been typeset from a  $\text{\TeX}/\text{\LaTeX}$  file prepared by the author.

This figure "wr0102c.png" is available in "png" format from:

<http://arxiv.org/ps/2204.09349v1>